Resonant tuning of Langevin transducers for ultrasonically assisted machining applications

V.K. Astashev[1], K.A. Pichugin[1], X. Li[2], A. Meadows[3], and V.I. Babitsky[3]

[1]Institute of Machine Studies, Russian Academy of Sciences, 101901, Malij Kharitonievsky, Moscow, Russia
[2]Centre for Medical and Industrial Ultrasonics (C-MIU), James Watt School of Engineering, University of Glasgow, Glasgow, G12 8QQ, UK
[3]Wolson School of Mechanical, Electrical and Manufacturing Engineering, Loughborough University, Loughborough, LE11 3TU, UK

Abstract — This paper provides a fundamental study into the trade-offs between the location of piezoceramic elements, resonant frequency, and achievable ultrasonic vibration amplitude at the working end of the Bolted Langevin-style Transducers (BLT) for Ultrasonically Assisted Machining (UAM) applications. Analytical models and Finite Element (FE) models are established for theoretical study, which are then validated by experiments on four real electro-mechanical transducers. Results suggest that resonant frequency and oscillation amplitude of the BLTs depend essentially on the dimensions of the system and the location of piezoceramic elements. The highest resonant frequency and the maximal vibration are achieved when the piezoceramic elements are at the longitudinal displacement node, where the highest effective electro-mechanical coupling coefficient value is exhibited. However, the minimal resonant frequency and the lowest vibration, which is almost equal to zero, are observed when the piezoceramic elements are located at the displacement anti-node. In addition, the longitudinal displacement node locations are dependent on the resonant frequency of the devices rather than the locations of the piezoceramic elements.

Index Terms—BLT transducer, EMA, FE, impedance, UAM

I. Introduction

Ultrasonically assisted machining (UAM) is implemented by superimposing a micro-scale high frequency vibration to the relative motion of a cutting tool tip to make the tool-workpiece interaction a discontinuous process [1], [2], [3]. Compared with the conventional machining process, UAM technology introduces benefits such as great reductions in machine-tool cutting force, torque, temperature, burr formation, improvement on the surface finish integrity and enhancement on the ability of machining difficult-to-cut materials [4]. Efficiency of the UAM process is mainly determined by the amplitude of the oscillations at the working end. Therefore, resonance regime needs to be implemented to ensure a maximal vibration amplitude is always maintained [5].

The UAM processes are normally facilitated with a Langevin-style ultrasonic transducer as the vibration generator, which consists of vibration exciters and rod wave conductors, transmitting the developed ultrasonic vibration to the tool. Piezoelectric vibration exciters are widely used in these transducers due to the advantages of small size and high mechanical quality, which generates less heat. However, one of the drawbacks of the piezoceramic material is the brittleness, which severely restrains the maximum capacity. In addition, piezoceramic exciters need a sufficient pre-stress to avoid the transducer parts becoming loose, and the resultant preliminary static stresses and strains will create limitations on the force and strains at high excitation levels.

Corresponding author: Dr. Xuan Li (email: Xuan.Li@glasgow.ac.uk Tel: (+44) (0)758 782 3718)

The traditional way to configure a Langevin-style transducer is to locate the piezoceramic exciters at the longitudinal displacement node so that the piezoceramic elements efficiency can be maximised [6], [7]. However, this configuration is impractical for transducer's fixture purpose during machining. This is because in most cases a flange needs to be introduced at the displacement node so that the transducer can be clamped in the chuck to minimise the vibration loss, which means the piezoceramic elements will have to be moved from the node.

As reported in [5], location of the piezoceramic exciters in the waveguide significantly affects the resonant frequency and oscillation amplitude, to investigate this, an analytical model is established with piezoceramic exciters at different positions of the waveguide to study the influence. FE models are also created, and several electro-mechanical transducers are manufactured to validate the theoretical results.

II. Analytical Model

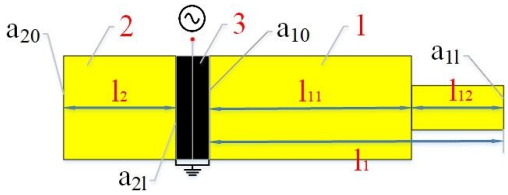

Fig. 1 Step rod system with a pair of piezoelectric exciters

Considering a step rod system which consists of two sections presented in **Fig. 1**: waveguide 1, which has a step shape to increase the vibration amplitude at the working end, with a length l_{11} for the thicker section and a length l_{12} for the thinner section, constituting an overall length l_1; waveguide 2, with a length l_2 . These two waveguides sandwich a stack of piezoceramic elements 3 rigidly. $l = l_1 + l_2 = l_{11} + l_{12} + l_2$ is the total length of the system. The thickness of the piezoelectric element is neglected.

An alternating voltage $v(t) = Ve^{j\omega t}$ with a magnitude V and an angular frequency ω is applied to the piezoceramic elements, where $j = \sqrt{-1}$. Due to the piezoelectric effect, the

piezoceramic elements will deform and interact with the rods which then causes the vibrations to propagate. At steady-state harmonic oscillation conditions, the relations between the electrical and mechanical oscillations of the piezoceramic elements are defined as [8], [9]:

$$\begin{aligned} F_0 &= Ka_0 + \Phi q \\ V &= \Phi a_0 + \frac{q}{C} \end{aligned} \tag{1}$$

Where F_0, a_0, q are the complex amplitudes of the forces, deformation (strain amplitude) and charge generated by the piezoceramic elements; K is the stiffness of the piezoceramic elements with a short-closed circuit; C is the capacity of piezoceramic elements without deformation; Φ is Mason's piezoelectric constant.

A. Dynamic equations

To describe the vibrations of the step rod system in **Fig. 1**, the system is dissected at the components interfaces. The force acting on the adjacent subsystems are equal in magnitude but opposite in direction:

$$\begin{aligned} f_{13} &= -f_{31} \\ f_{32} &= -f_{23} \end{aligned} \tag{2}$$

The oscillation at the cross section x for rod i, $(i = 1,2)$ can be defined as:

$$u_{ix}(t) = a_{ix}e^{j\omega t} \tag{3}$$

Where a_{ix} is the complex amplitude, and a_{10}, a_{1l} and a_{2l} of rod 1 and rod 2 are of interest, which can be defined as:

$$\begin{aligned} a_{10} &= F_{31}L_{00}^{(1)} \\ a_{1l} &= F_{31}L_{0l}^{(1)} \\ a_{2l} &= F_{32}L_{ll}^{(2)} \\ a_{20} &= F_{32}L_{l0}^{(2)} \end{aligned} \tag{4}$$

Where F_{ij} are the complex amplitudes of the forces presented in (2), $L_{sr}^{(i)} = L_{sr}^{(i)}(j\omega)$ is the dynamic compliance [10], which describes the complex amplitudes of oscillations of section r of the rod i ($i = 1, 2$) with the force acting in section s of the rod.

Using equation (4), the deformation of the package of the piezoceramic elements can be derived as:

$$na_0 = a_{10} - a_{2l} = F_{31}L_{00}^{(1)} - F_{32}L_{ll}^{(2)} \tag{5}$$

Where n is the number of piezoceramic elements.

From equation (1), the relation between the generated force and vibration of the piezoceramic elements is:

$$F_0 = \Phi CV + K_1 a_0 \tag{6}$$

Where $K_1 = K - C\Phi^2$ is the stiffness of the piezoceramic elements with an open circuit.

Taking the mass of the piezoceramic elements $m_3 = nm$ (m is the mass of one piezoelement) into account, at steady-state oscillations:

$$\begin{aligned} F_{13} + F_{23} &= -m_3 a_3 \omega^2 \\ F_{13} - F_{23} &= 2F_0 \end{aligned} \tag{7}$$

Where $a_3 = (a_{10} + a_{2l})/2$ is the complex amplitude of the oscillations at the center of the package of the piezoceramic elements.

From equations (1) and (4) to (7), the expressions of the strain amplitude of the piezoceramic elements and the force developed are:

$$\begin{aligned} a_0 &= -4\Phi CV \frac{\left(L_{00}^{(1)} + L_{ll}^{(2)}\right) + m_3\omega^2 L_{00}^{(1)} L_{ll}^{(2)}}{4 + \frac{4K_1}{n}\left(L_{00}^{(1)} + L_{ll}^{(2)}\right) + m_3\omega^2\left(L_{00}^{(1)} + L_{ll}^{(2)} + \frac{4K_1}{n}L_{00}^{(1)}L_{ll}^{(2)}\right)} \\ F_0 &= \Phi CV \frac{4 + m_3\omega^2\left(L_{00}^{(1)} + L_{ll}^{(2)}\right)}{4 + \frac{4K_1}{n}\left(L_{00}^{(1)} + L_{ll}^{(2)}\right) + m_3\omega^2\left(L_{00}^{(1)} + L_{ll}^{(2)} + \frac{4K_1}{n}L_{00}^{(1)}L_{ll}^{(2)}\right)} \end{aligned} \tag{8}$$

Combining equation (1) and (6) to (8), the charge generated on the piezoceramic elements is:

$$q = CV \frac{4 + \frac{4K}{n}\left(L_{00}^{(1)} + L_{ll}^{(2)}\right) + m_3\omega^2\left(L_{00}^{(1)} + L_{ll}^{(2)} + \frac{4K}{n}L_{00}^{(1)}L_{ll}^{(2)}\right)}{4 + \frac{4K_1}{n}\left(L_{00}^{(1)} + L_{ll}^{(2)}\right) + m_3\omega^2\left(L_{00}^{(1)} + L_{ll}^{(2)} + \frac{4K_1}{n}L_{00}^{(1)}L_{ll}^{(2)}\right)} \tag{9}$$

The excitation force amplitudes for the rods are:

$$\begin{aligned} F_{31} &= -2\Phi CV \frac{2 + m_3\omega^2 L_{ll}^{(2)}}{4 + \frac{4K_1}{n}\left(L_{00}^{(1)} + L_{ll}^{(2)}\right) + m_3\omega^2\left(L_{00}^{(1)} + L_{ll}^{(2)} + \frac{4K_1}{n}L_{00}^{(1)}L_{ll}^{(2)}\right)} \\ F_{32} &= -2\Phi CV \frac{2 + m_3\omega^2 L_{00}^{(1)}}{4 + \frac{4K_1}{n}\left(L_{00}^{(1)} + L_{ll}^{(2)}\right) + m_3\omega^2\left(L_{00}^{(1)} + L_{ll}^{(2)} + \frac{4K_1}{n}L_{00}^{(1)}L_{ll}^{(2)}\right)} \end{aligned} \tag{10}$$

When using the above equations for the step rods in **Fig. 1**, it is important to observe that rod 1 consists of a step geometry, so the dynamic compliance is:

$$\begin{aligned} L_{00}^{(1)} &= L_{00}^{(11)} - \frac{L_{0l}^{(11)}L_{l0}^{(11)}}{L_{ll}^{(11)} + L_{00}^{(12)}} \\ L_{0l}^{(1)} &= \frac{L_{0l}^{(11)}L_{0l}^{(12)}}{L_{ll}^{(11)} + L_{00}^{(12)}} \end{aligned} \tag{11}$$

Where the top index (11) and (12) denote the 1st and 2nd step of rod 1. Dynamic compliance expressions can be found in [2]:

$$\begin{aligned} L_{00}^{(11)}(j\omega) &= L_{ll}^{(11)}(j\omega) \\ L_{00}^{(1i)}(j\omega) &= -\frac{1}{w_{1i}\omega} \cdot \frac{\cos\xi_{1i} - j\frac{\psi}{4\pi}(\cos\xi_{1i} - \xi_i \sin\xi_{1i})}{\sin\xi_{1i} - j\frac{\psi}{4\pi}\xi_{1i}\cos\xi_{1i}} \\ L_{0l}^{(1i)}(j\omega) &= -\frac{1}{w_{1i}\omega} \cdot \frac{1 - j\frac{\psi}{4\pi}}{\sin\xi_{1i} - j\frac{\psi}{4\pi}\xi_{1i}\cos\xi_{1i}} \\ L_{ll}^{(2)}(j\omega) &= -\frac{1}{w_2\omega} \cdot \frac{\cos\xi_2 - j\frac{\psi}{4\pi}(\cos\xi_2 - \xi_2\sin\xi_2)}{\sin\xi_2 - j\frac{\psi}{4\pi}\xi_2\cos\xi_2} \end{aligned} \tag{12}$$

Where $i = 1, 2$, representing the number of the 1st and 2nd step in rod 1; $\xi_{1i} = \omega l_{1i}/c$; $\xi_2 = \omega l_2/c$; $c = \sqrt{E/\rho}$ is the speed of sound in the rod material. E, ρ and ψ are the Young's modulus, density and scattering coefficient of the rod material. $w_{11} = w_2 = S\sqrt{E\rho}$, $w_{12} = S_{12}\sqrt{E\rho}$ are the wave resistance of the 1st step of rod 1 and rod 2, and 2nd step of rod 1, respectively. S and S_{12} are the cross-sectional areas of the rod's thicker and thinner sections.

B. Dynamic characteristics

The relations of equation (1) to (12) allow us to study the dynamic behavior of the step rod system. $\xi = \xi_1 + \xi_2 = \xi_{11} + \xi_{12} + \xi_2 = \omega l/c$ is a dimensionless frequency. Assuming the length of the thinner step of rod 1 is $l_{12} = l/4$, and the piezoelectric elements are located within the thicker section of the rod length $l_{11} + l_2$. A dimensionless parameter $\lambda = l_2/(l_2 + l_{11})$ is introduced to determine the location of the piezoceramic elements.

The piezoceramic elements' material is PZT-4 Navy type I and the properties are presented in Table I [11]. There are two piezoceramic elements in parallel in the step rod system. The rod material is Aluminium 6082 alloy, with a density $\rho = 2710\ \mathrm{kg/m^3}$, Young's modulus $E = 71\ \mathrm{GPa}$, and scattering coefficient $\psi = 0.0375$. The dimensions of the step rod system are that the thicker section diameter is 50 mm and the thinner section diameter is 30 mm. $l_{12} = 60$ mm and $l_2 + l_{11} = 180$ mm. The applied voltage amplitude to the piezoceramic elements is 1 V.

TABLE I
PZT-4 NAVY TYPE I PIEZOCERAMIC MATERIAL PROPERTIES

Outer diameter [mm]	50
Inner diameter [mm]	19
Thickness [mm]	6
Density ρ [kg/m^3]	7600
Poisson ratio	0.31
Relative permittivity ε_{11}^{T}	1470
Relative permittivity ε_{33}^{T}	1470
Relative permittivity ε_{33}^{S}	731
Permittivity of free space ε_0 [F/m]	8.85×10^{-12}
Piezoelectric charge coefficient d_{31} [C/N]	-1.32×10^{-10}
Piezoelectric charge coefficient d_{33} [C/N]	3.15×10^{-10}
Piezoelectric charge coefficient d_{15} [C/N]	5.11×10^{-10}
Elastic compliance coefficient S_{11}^{E} [m^2/N]	1.27×10^{-11}
Elastic compliance coefficient S_{33}^{E} [m^2/N]	1.56×10^{-11}
Mechanical quality factor Q	600
Mason's constant Φ [N/C]	3.45×10^{9}
Stiffness K [N/m]	2.1×10^{10}
Capacitance C [F]	4.23×10^{-9}

Driven at the 2nd longitudinal mode, the resonant frequency and the working end vibration amplitude as a function of λ are presented in **Fig. 2**. BS, NP, FS and AN refer to piezoceramic elements located at longitudinal displacement Back Section, Nodal Point, Front Section, and Anti-Node. The maximum resonant frequency value is observed when $\lambda \approx 0.33$, corresponding to the piezoceramic elements located roughly at the quarter length of the rod system counting from the left-hand side in **Fig. 1**, where the displacement node position is. The resonant frequency drops as the piezoceramic elements deviate away from the node. The minimum resonant frequency value is exhibited when $\lambda \approx 0.67$, meaning that the piezoceramic elements are at around the geometrical centre of the step rod system, where the displacement anti-node is.

For the mechanical and electrical characteristics of the step rod system, the working end oscillation amplitude and the developed current reach to the maximal values when the piezoceramic elements are at the displacement node, in other words, the electrical resonance and mechanical resonance coincide. However, an extremely low current level when the piezoceramic elements are at displacement anti-node results in a low energy transfer therefore hardly any mechanical vibration developed at the transducer's working end.

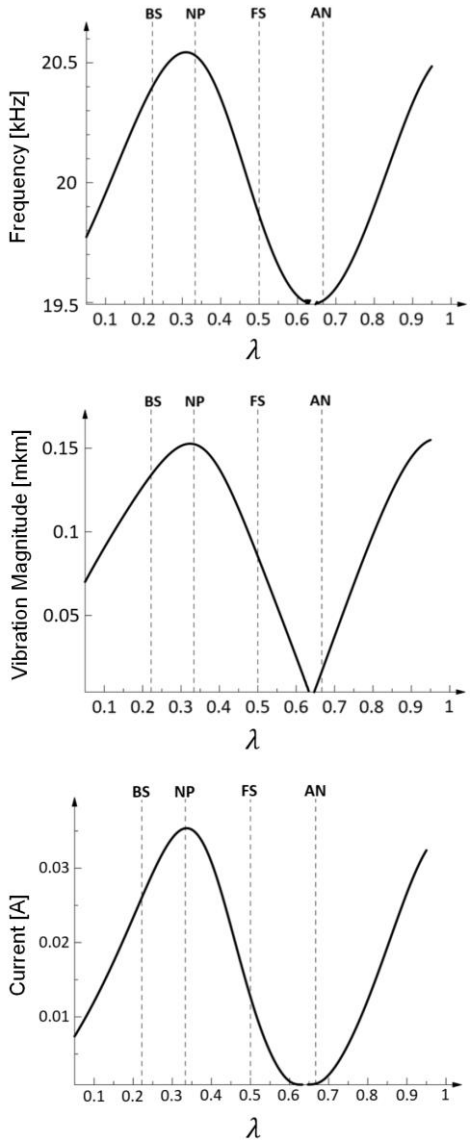

Fig. 2 Resonant frequency, vibration amplitude and electrical current dependence on parameter λ

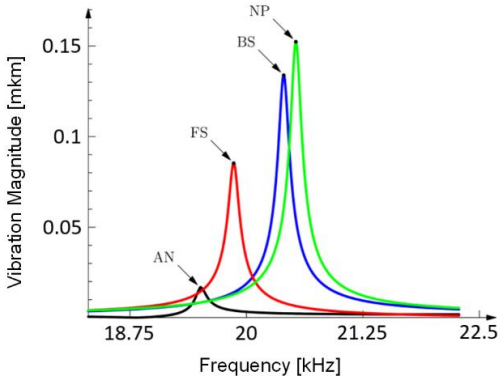

Fig. 3 Amplitude-frequency characteristics of the step rod system working end of different transducer configurations

Fig. 3 presents the amplitude-frequency characteristics of the step rod system's working end oscillations, excited at the 2nd longitudinal mode with a 1 V applied voltage, when the piezoceramic elements located at BS, FS, NP and AN respectively.

Results show that the maximal amplitude occurs when the piezoceramic elements are at the displacement node, and then the amplitude drops when the piezoceramic elements shift away from the node. The minimal amplitude, which is close to zero, appears if piezoelectric elements are at the anti-node. Another observation is the high mechanical quality of the NP system, which will present the highest efficiency in preserving mechanical energy. However, the high quality can impede practical implementation of the resonant modes due to high sensitivity of the regimes to small changes in system parameters and excitation, which is likely to incur the 'jump' phenomenon that has been discovered by a number of experiments in [12].

III. Langevin Transducer

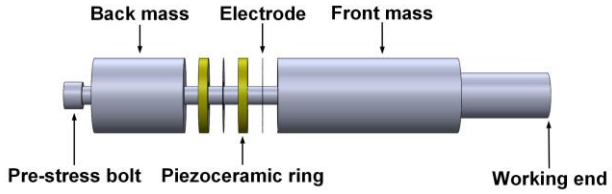

Fig. 4 Exploded view of a step shape BLT transducer

The ultrasonic transducers used in this research are standard Bolted Langevin-style Transducers (BLT), which are employed to represent the step rod system in **Fig. 1**. This type of transducer consists of a stack of piezoceramic elements sandwiched between a back mass and a front mass, presented in **Fig. 4**. In this case, the piezoceramic elements are located at the displacement node and the full wavelength step shape ultrasonic transducer is operated at its 2nd longitudinal mode at around 20 kHz.

The front mass and back mass material is Aluminum 6082 alloy. The electrode is made from copper, and the torque bolt, which is used to pre-stress the transducer components, is made of tool steel. The material properties are presented in Table II.

TABLE II
Ultrasonic Transducer's Material Properties

Material	Aluminium	Tool Steel	Copper
Density [kg/m^3]	2710	7860	8900
Young's modulus [GPa]	71	203	110
Poisson's ratio	0.33	0.285	0.37

The fabricated BLT transducers with piezoceramic elements at different locations are illustrated in **Fig. 5**.

During transducers fabrication process, the components were pre-stressed by a bolt to compensate the low tensile strength of the piezoceramic rings, therefore avoiding transducer's failure during high power applications [13].

The length of the transducers is around 250 mm, which roughly equals the full wavelength of ultrasound when the devices are operated at the 2nd longitudinal modes at around 20 kHz. The working end diameter of the transducers is 30 mm, recessing from a 50 mm diameter piezoceramic exciters with a step shape. The theoretical vibration amplification gain of the ultrasonic vibration is calculated as 2.78 [2].

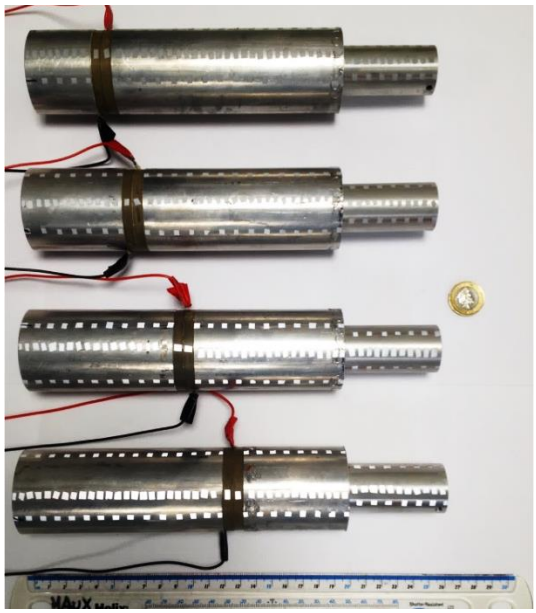

Fig. 5 BLT transducers with piezoceramic elements at BS, NP, FS, AN (top to bottom)

IV. Dynamic Characterisation

A. Eigen-frequencies and eigen-modes

To characterise the ultrasonic transducers' modal responses, experimental modal analysis (EMA) was conducted. EMA is a data acquisition and visualisation process, which employs the experimentally-obtained frequency response functions (FRF) to capture the modal parameters (modal frequency, modal damping, and mode shape) [14]. To excite the transducers, a forced excitation is used with a flat power spectrum across the frequency band of interest [15], which is set as 0 kHz to 50 kHz, to capture the dynamic behaviors at around 20 kHz.

The excitation signal is generated by a generator (Data Physics Quattro) and then amplified by a power amplifier (QSC RMX 4050HD), before being supplied to the ultrasonic transducers. A 3-D laser vibrometer (Polytec CLV-3000) is used to capture the vibrational velocities at a number of grid points on the transducers surface. Data acquisition and processing software (SignalCalc, Data Physics) are adopted to calculate the FRFs from the input and output signals of the transducers and to apply curve-fitting routines to extract the modal frequencies, magnitudes and phase data. The velocity data on ultrasonic transducers surface points are then exported to the modal analysis software (ME'scopeVES, Vibrant Technology Inc), to extract the eigen-modes.

To compare with the predicted vibration mode shapes in the FE models, experimentally extracted mode shapes of the ultrasonic transducers operated at the 2nd longitudinal modes at around 20 kHz are presented in **Fig. 6**.

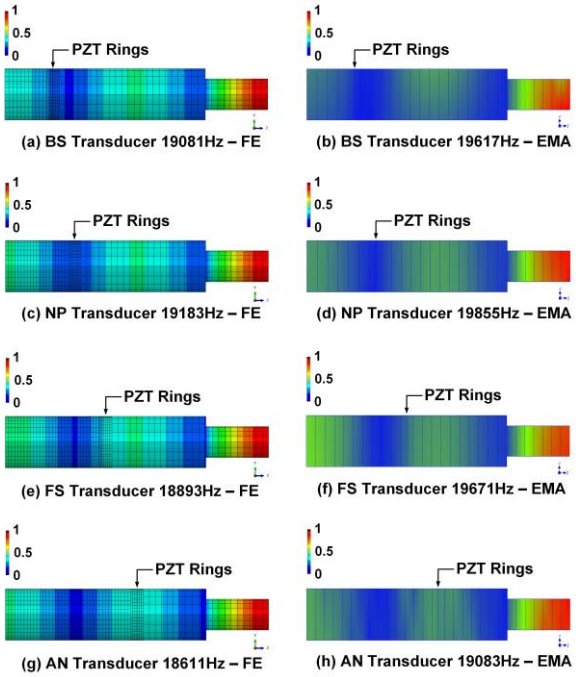

Fig. 6 FE vs EMA of the normalised 2nd longitudinal modes of the transducers

All transducers show two displacement nodes, one of which is located at the step interface, and the other remains at approximately the quarter length of the transducers from the back mass face. This indicates that the locations of the displacement node and anti-node are related to the operating frequency of the device, rather than the position of the piezoceramic elements.

TABLE III
TRANSDUCER'S RESONANT FREQUENCIES - FE VS EMA

Configuration	BS	NP	FS	AN
FE [Hz]	19081	19183	18893	18611
EMA [Hz]	19617	19855	19671	19083
Error	2.8%	3.5%	4.1%	2.5%

Resonant frequencies of the transducers are presented in Table III. The good correlation in terms of the mode shapes and resonant frequencies between the FE and EMA results suggest that these models can capture the vibrational behaviour of the transducers.

B. Impedance

In addition to the analysis of the mechanical behaviour, the electrical characteristics are also studied.

In FE models, the impedance is extracted by calculating the derivative of the charge generated at piezoceramic elements surfaces and then dividing by the applied voltage. During experiments, the impedance curves of the transducers were measured with an impedance analyser (Agilent 4294A).

The predicted electrical impedances and phase in FE and experimental measurements are presented in **Fig. 7** and **Fig. 8**.

From **Fig. 7**, the predicted impedance-frequency curves in FE models (in blue) present a similarity to the measured characteristics (in red), although the variations in resonant

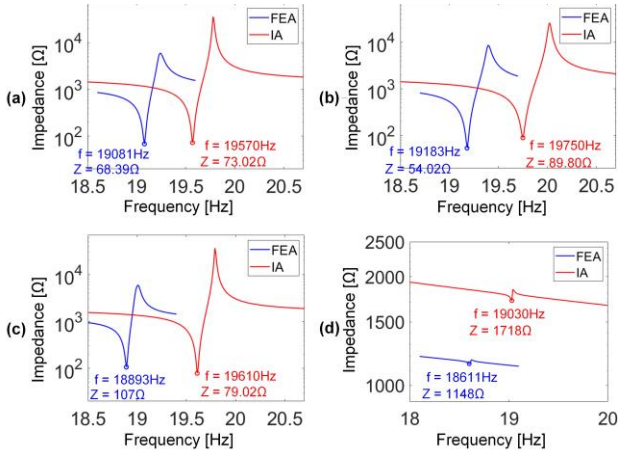

Fig. 7 Impedance of the transducers with piezoceramic rings are at: (a) BS, (b) NP, (c) FS, (d) AN

frequency and impedance value. Compared with the BS, NP and FS transducers responses, the AN transducer presents a peculiar response, in terms of extremely high impedance levels, indistinctive resonance and anti-resonance.

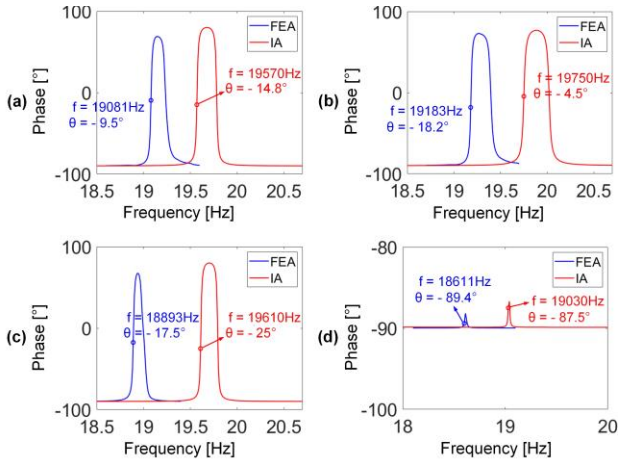

Fig. 8 Phase of the transducers with piezoceramic rings are at: (a) BS, (b) NP, (c) FS, (d) AN

From the phase-frequency curves shown in **Fig. 8**, the predicted results in FE models (in blue) resemble the measured phase (in red), with respect to the 'bell shape' and the phase values for the BS, NP and FS transducers. However, the AN transducer demonstrates an extremely small change in the phase across the resonant frequency, whose value remains at around -90°. This means that the AN transducer will present a purely capacitive characteristic at the 2nd longitudinal mode, which will result in an almost zero-energy transfer.

The peculiar responses of the AN transducer impedance and phase is due to the low stress and strain when the piezoceramic elements are located at the anti-node, which in turn, generates a low force from the piezoceramic elements, causing the device to have a low vibration.

In addition, the BLT devices are normally comprised of multiple half-wavelength resonators, therefore if dissecting the AN transducer in **Fig. 6** at the anti-node, the half-wavelength resonator of the AN transducer will locate the piezoceramic

elements at one end of the metal mass, causing an asymmetric structure distribution and resulting in a high acoustic impedance. As a comparison, the half-wavelength resonator of the NP transducer will locate the piezoceramic elements at the centre of the metal mass, and result in an acoustic balance.

To evaluate the energy conversion rate from the electrical source to mechanical vibration, coupling coefficients of the transducers are calculated from FE models and experiments, based on [16]:

$$K_{eff} = \sqrt{\frac{f_a^2 - f_r^2}{f_a^2}} \quad (8)$$

Where f_a is the anti-resonant frequency and f_r is the resonant frequency. Results of the coefficients are presented in Table IV.

TABLE IV
TRANSDUCER'S ELECTROMECHANICAL COUPLING COEFFICIENTS

FE prediction	**BS**	**NP**	**FS**	**AN**
f_r [Hz]	19081	19183	18893	18611
f_a [Hz]	19240	19394	19007	18621
$Z_{e\,min}$ [Ω]	68.39	54.02	107	1148
$Z_{e\,max}$ [Ω]	5961	8520	5954	1177
K_{eff}	**0.1283**	**0.1471**	**0.1094**	**0.0328**
Phase	- 9.5°	- 18.2°	- 17.5°	- 89.4°
Measurements	**BS**	**NP**	**FS**	**AN**
f_r [Hz]	19570	19750	19610	19030
f_a [Hz]	19780	20020	19790	19040
$Z_{e\,min}$ [Ω]	73.02	89.80	79.02	1718
$Z_{e\,max}$ [Ω]	35890	25880	36640	1845
K_{eff}	**0.1453**	**0.1637**	**0.1346**	**0.0324**
Phase	- 14.8°	- 4.5°	- 25.0°	- 87.5°

The NP transducer presents the highest coefficient values, which suggests that this transducer will exhibit the highest energy conversion rate. As the piezoceramic elements move away from the node, the value slightly drops. The coefficient value reaches nearly to zero when the piezoceramic elements are at the anti-node, which indicates a zero-energy transfer into mechanical vibration.

C. *Dynamic vibration response*

In order to study the dynamic response of the ultrasonic transducers at escalated power levels, harmonic excitation experiments were performed.

Frequency sweeps are used to drive the transducers with a range centring the transducers 2nd longitudinal resonant frequencies. A burst sinusoidal signal is generated from a signal generator (Agilent 33210A Function/Arbitrary Waveform Generator, 10 MHz), which is then boosted by a power amplifier unit (HFVA-62), before being supplied to excite the transducers. The developed vibration signals are captured with a 1-D laser doppler vibrometer (OFV-303 Polytec) at the working end of the transducers. The electrical information, such as applied voltage and developed current are extracted from the power amplifier's output. These signals are monitored and recorded using an oscilloscope (PicoScope 4424), and then processed using data acquisition hardware and interface (BNC-2110, National Instruments) in conjunction with a LabView program, to calculate the transducer's acoustic power, current and phase angle.

The range of excitation voltage levels is from 1 V_{rms} to 100 V_{rms}, with an increment of 10 V_{rms}.

1) *Vibration response*

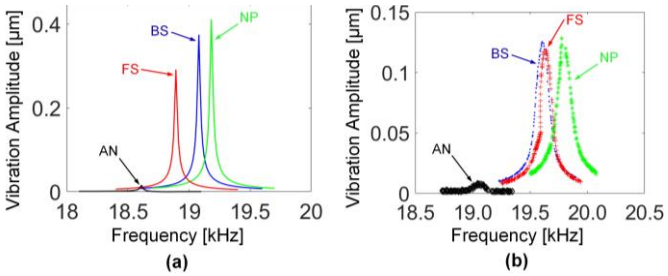

Fig. 9 Amplitude-frequency characteristics at the transducers working end with 1 V_{rms} input voltage: (a) FE prediction, (b) experimental measurements

The amplitude-frequency curves at the transducers working end with a 1 V_{rms} applied voltage are presented in **Fig. 9**.

Both the FE predicted results and the experimental measurements show that the NP transducer demonstrates a higher resonant frequency value, and as the piezoceramic elements deviate away from the node, resonant frequency decreases, which is consistent to the conclusions in [7], and most importantly, matches to the results of the analytical models in **Fig. 3**.

In terms of the vibration, the NP transducer develops the maximal vibration amplitude. The AN transducer, however, develops an extremely low level of vibration. BS and FS transducers show lower amplitudes than NP transducer, but significantly higher than that of the AN transducer. These observations are consistent with the analytical results in **Fig. 3**.

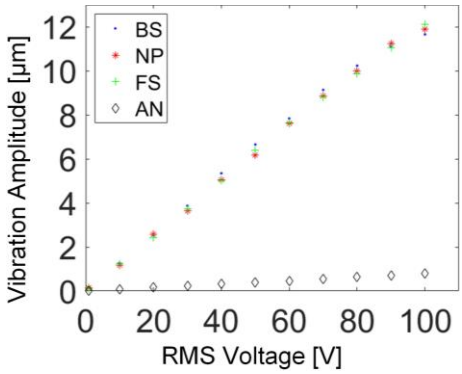

Fig. 10 Vibration amplitude vs applied voltage: (a) BS, NP and FS transducers, (b) AN transducer

The vibration amplitude of the transducers excited at a voltage from 1 V_{rms} to 100 V_{rms} are presented in **Fig. 10**.

The amplitude increases to around 12 μm zero-to-peak as the applied voltage increase to 100 V_{rms} for the BS, FS and NP transducers. However, the response of AN transducer demonstrates an extremely low level, with a maximal amplitude of 0.8 μm zero-to-peak at a 100 V_{rms} voltage. These results are consistent with the trend in **Fig. 3** and **Fig. 9**.

2) Electrical current and acoustic power

In addition to the mechanical vibration response of the transducers excited at escalated power levels, electrical current and power consumption are also studied.

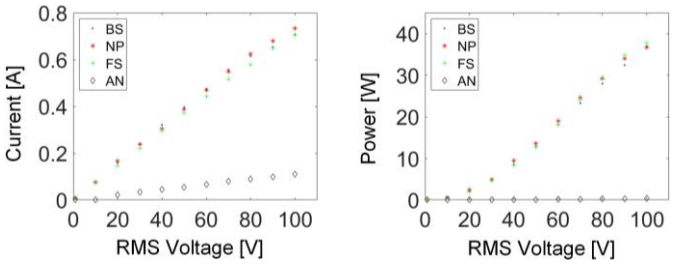

Fig. 11 Electrical current and power vs applied voltage

Incorporating the phase angles between the applied voltage and developed current in the piezoceramic elements, the active power can be calculated. Results of the electrical current and power are presented in **Fig. 11**.

For the BS, NP and FS transducers, current and power show a comparable level, with maximal values around 0.75 A and 38 W at a 100 V_{rms} applied voltage. Even if excited at the highest voltage level, however, the AN transducer can hardly develop any current and power, with values of no more than 0.12 A and 0.4 W. This is due to the extremely high impedance values and an almost -90° phase angle presented in **Fig. 7** and **Fig. 8**, which leads to a poor mechanical behaviour for this type of transducer.

3) Waveform

To explore the structural vibration response of the transducers excited at the 2nd longitudinal mode, waveforms are extracted from FE models and experiments. The excitation voltage to piezoceramic rings is 1 V_{rms}. Results are shown in **Fig. 12**.

Despite the difference in the predicted amplitude in the FE models and the recorded amplitude in experiments, both sets of results demonstrate that the nodes locations are at roughly at a 60 mm away from both ends of the transducers, in other words, at a quarter wavelength of end faces of the devices, which is consistent with the observations in **Fig. 6**.

The vibration amplitude of the AN transducer show a significant lower level compared to the other three configurations as a result of the high impedance and the -90° phase angle at resonance.

The amplification gain values calculated from the FE models and experiments are presented in Table V, which have a good agreement with the theoretically calculated gain value 2.78.

TABLE V
VIBRATION AMPLIFICATION GAIN VALUES THEORY VS EXPERIMENT

Configuration	FE	Experiment
BS	2.89	2.66
NP	2.88	2.79
FS	2.90	2.73
AN	2.96	2.85

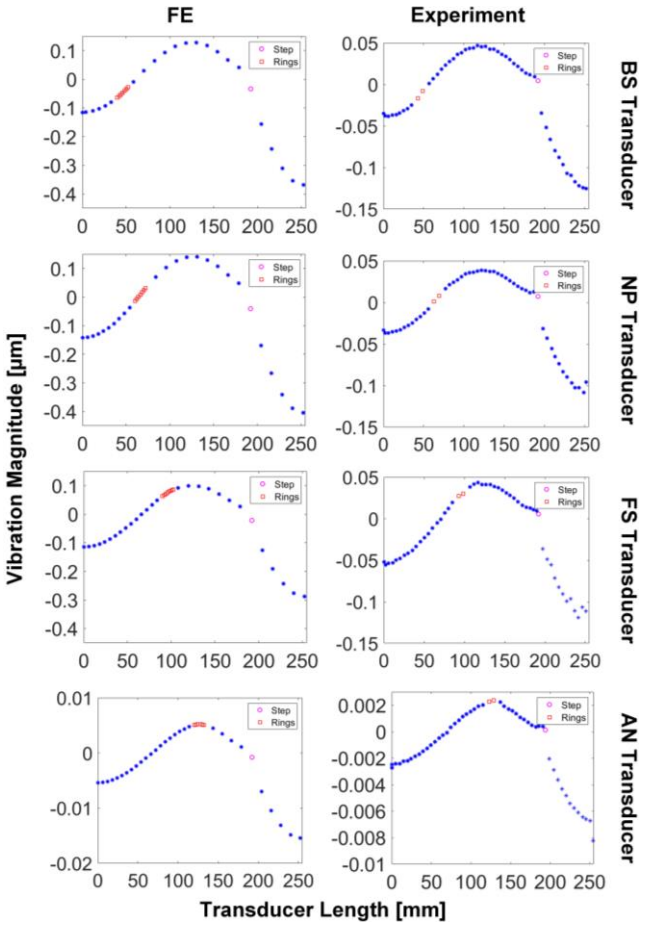

Fig. 12 Transducers waveforms driven at the 2nd longitudinal mode with a 1 V_{rms} applied voltage

V. Conclusion

This paper presents the scientific findings of the trade-offs between the locations of the piezoceramic elements, resonant frequency, and achievable ultrasonic vibration amplitude at the BLT transducers' working end.

Results show that the resonant frequency and vibration amplitude of the BLTs depend essentially on the location of the piezoceramic elements. The highest resonant frequency and the maximal vibration amplitude are achieved when piezoceramic elements are at the displacement node for the analytical models, FE models and real electro-mechanical transducers. The minimal vibration is observed for the AN transducer which almost equals zero, even if driven at a high excitation level.

Location of the displacement nodes is determined by the resonant frequency and operating mode of the BLTs, which remains a constant despite the change of the location of piezoceramic elements.

For machining applications, a proper design of a BLT transducer must avoid locating the piezoceramic elements at the displacement anti-node. To achieve the highest vibration amplitude at the tool tip whilst ensures the stress level to stay below the material yield strength, the position of piezoceramic elements needs to be carefully adjusted.

ACKNOWLEDGEMENT

The work of the authors from the Institute of Machine Studies was supported by a grant from the Russian Science Foundation (project No 19-19-065).

The authors acknowledge the impedance analyzer and laser vibrometers facilities in the Centre for Medical and Industrial Ultrasonics (C-MIU) at the University of Glasgow.

REFERENCES

[1] J. Kumabe, "Vibration Cutting (in Japanese), " *Tokyo: Jikkyou Publishing Co*, 1979.

[2] V. K. Astashev and V. I. Babitsky, "Ultrasonic Processes and Machines, " *Dynamics, Control and Applications, Berlin: Springer-Verlag*, 2007.

[3] W. X. Xu and L. C. Zhang, "Ultrasonic vibration-assisted machining: principle, design and application," *Advanced Manufacturing*, vol. 3, no. 3, pp. 173-192, 2015.

[4] S. Voronina, V. Babitsky, and A. Meadows, "Modelling of autoresonant control of ultrasonic transducer for machining applications," *Proceedings of Institute of Mechanical Engineering Part C: Journal of Mechanical Engineering Science*, vol. 222, no. 10, pp. 1957-1974, 2008.

[5] V. K. Astashev and K. A. Pichygin, "Resonance adjustment and optimization of parameters of an ultrasonic rod system with a piezoelectric vibration exciter," *Journal of Machinery Manufacture and Reliability*, vol. 42, no. 5, pp. 347-352, 2013.

[6] S. Lin and F. Zhang, "Study of vibrational characteristics for piezoelectric sandwich ultrasonic transducers," *Ultrasonics*, vol. 32, no. 1, pp. 39-42, 1994.

[7] S. Lin, "Optimization of the performance of the sandwich piezoelectric ultrasonic transducer," *The Journal of the Acoustical Society of America*, vol. 115, no. 1, pp. 182-186, 2004.

[8] A. A. Kharkevich, "Theory of electroacoustic converters (Izbrannye trudy, in Russian), " Vol. 1. *Moscow: Nauka*, 1973.

[9] A. V. Rimsky-Korsakov, "Electroacoustics (in Russian), " *Communication*, 1973.

[10] V. I. Babitsky, "Theory of vibro-impact sytems and applications, " *Berlin: Springer-Verlag*, 1998.

[11] D. Berlincourt, H. Krueger, and C. Near, "Properties of Morgan electro ceramic ceramics," *Technical Publication TP-226,Properties of Piezoelectricity Ceramics*, pp. 1-12, 2000.

[12] A. Mathieson, A. Cardoni, N. Cerisola, and M. Lucas, "The influence of piezoceramic stack location on nonlinear behavior of Langevin transducers," *IEEE Transactions on Ultrasonics, Ferroelectrics, and Frequency Control*, vol. 60, no. 6, pp. 1126-1133, 2013.

[13] E. Riera, A. Cardoni, A. Blanco, V. Acosta, and J. Gallego-Juárez, "Characterising the nonlinear dynamics of power ultrasonic systems," *Internoise 2010, noise and sustainability*, no. 43, pp. 1-10, 2012.

[14] P. Avitabile, "Experimental Modal Analysis," *Modal Analysis and Controls Laboratory, University of Massachusetts Lowell, raft document for Sound & Vibration Magazine,* vol. 35, no. 1, pp. 1-15, 2001.

[15] H. Al-Budairi, "Design and analysis of ultrasonic horns operating in longitudinal and torsional vibration," *University of Glasgow, School of Engineering, Enlighten PhD Theses,* December, 2012.

[16] A. Caronti, R. Carotenuto, and M. Pappalardo, "Electromechanical coupling factor of capacitive micromachined ultrasonic transducers," *The Journal of Acoustical Society of America*, vol. 113, no. 1, pp. 279-288, 2003.